PHYSICAL REVIEW B **90**, 041109(R) (2014)

Magnetic structure of GdBiPt: A candidate antiferromagnetic topological insulator

R. A. Müller,[1] N. R. Lee-Hone,[2] L. Lapointe,[1] D. H. Ryan,[2] T. Pereg-Barnea,[2] A. D. Bianchi,[1]
Y. Mozharivskyj,[3] and R. Flacau[4]

[1]*Département de Physique, Université de Montréal, Montréal, QC, Canada*[*]
[2]*Department of Physics, McGill University, 3600 University St., Montréal, QC, Canada*[*]
[3]*Department of Chemistry and Chemical Biology McMaster University, Hamilton, ON, Canada*
[4]*Canadian Neutron Beam Centre, Chalk River Laboratories, ON, Canada*

(Received 30 January 2014; published 28 July 2014)

A topological insulator is a state of matter which does not break any symmetry and is characterized by topological invariants, the integer expectation values of nonlocal operators. Antiferromagnetism, on the other hand, is a broken symmetry state in which the translation symmetry is reduced and time reversal symmetry is broken. Can these two phenomena coexist in the same material? A proposal by Mong *et al.* [Phys. Rev. B **81**, 245209 (2010)] asserts that the answer is yes. Moreover, it is theoretically possible that the onset of antiferromagnetism enables the nontrivial topology since it may create spin-orbit coupling effects which are absent in the nonmagnetic phase. The current work examines a real system, half-Heusler GdBiPt, as a candidate for topological antiferromagnetism. We find that the magnetic moments of the gadolinium atoms form ferromagnetic sheets which are stacked antiferromagnetically along the body diagonal. This magnetic structure may induce spin-orbit coupling on band electrons as they hop perpendicular to the ferromagnetic sheets.

DOI: 10.1103/PhysRevB.90.041109 PACS number(s): 75.25.−j, 75.50.Ee, 73.20.−r

The discovery of the quantum Hall effect (QHE) [1] led to a new way of classifying matter—a phase transition does not have to be bound to spontaneous symmetry breaking. Two years after von Klitzing's discovery, Thouless, Kohmoto, Nightingale, and den Nijs (TKNN) [2] developed the concept of topological invariants in their description of the same effect. The TKNN number represents the topology of the system in the form of an integral of the Bloch wave functions over the Brillouin zone. This nonlocal operation results in an integer number which also corresponds to the number of dissipationless edge modes. The edge modes are guaranteed by the topology and are also protected by it. The TKNN number, however, explicitly breaks time reversal symmetry and is therefore zero in a time reversal invariant system.

In 2005, Kane and Mele [3] proposed a new state of matter: a topological system which does not break time reversal (TR) symmetry. In their example, the topological number is defined modulo 2 and the edge modes give rise to the quantum spin Hall effect. Many exciting developments have been presented since, both experimentally and theoretically, but many questions still remain [4–6]. One such question is whether the topological order can coexist with a broken symmetry state. Moreover, is it possible for a local order parameter which breaks one or more symmetries to give rise to topological order? The answer to this question, theoretically, is a tentative "yes" [7,8].

In 2010 Mong *et al.* [7] came forward with the concept of an antiferromagnetic topological insulator (AFTI). In contrast to an *ordinary* topological insulator, in an AFTI the presence of magnetic order breaks TR symmetry Θ as well as primitive-lattice translational symmetry $T_{1/2}$, yet their product $S = \Theta T_{1/2}$ is preserved. This allows the definition of a topological invariant which preserves the S symmetry. In three dimensions the result is a topological state with antiferromagnetic order. Depending on whether the surface breaks the S symmetry or not, metallic surface states may arise within the band gap and a half-integer quantum Hall effect is expected [7]. Moreover, in certain systems, the presence of the topological phase is bound to the antiferromagnetic phase and so vanishes above the Néel temperature. This makes the AFTI particularly interesting, as the topological state appears only after the system undergoes a classical phase transition. Therefore, changing the temperature allows one to turn the topological state on and off resulting in a quantum phase transition at T_N. Mong *et al.* [7] propose in their "model B" that the spin-orbit interaction may result from the Néel order. Their model contains itinerant electrons and fixed spins. When the electrons hop between lattice sites they may do so through intermediate magnetic sites. For certain paths of the conduction electrons the magnetic moments serve to create an Aharonov-Bohm-like flux which in turn acts as Rashba spin-orbit coupling, responsible for the topological order. The theoretical model is inspired by systems like GdBiPt which have been proposed to be topological based on first-principles calculations [9–11]. In order for the S symmetry to be preserved together with a significant spin-orbit coupling the model requires a specific magnetic structure. The moments should be aligned ferromagnetically in layers which are stacked antiferromagnetically. For the system to be gapped, the hopping between layers should be larger than the hopping within the layer. For the half-Heusler structure, this spin-orbit term is maximal if the moments are aligned ferromagnetically in the (111) plane and stacked antiferromagnetically along the [111] space diagonal as shown in Fig. 1 [7]. The Heusler and the derivative half-Heusler structures favor half-metallic band structures with just one band crossing at the Fermi level, while leaving all the other bands well separated, and have been also proposed as candidate materials for *conventional* topological insulators [9,12]. The purpose of the current work is to test whether the desired magnetic structure does indeed occur in GdBiPt. We report on powder neutron scattering measurements of GdBiPt which

[*]Also at Regroupement Québécois sur les Matériaux de Pointe (RQMP).

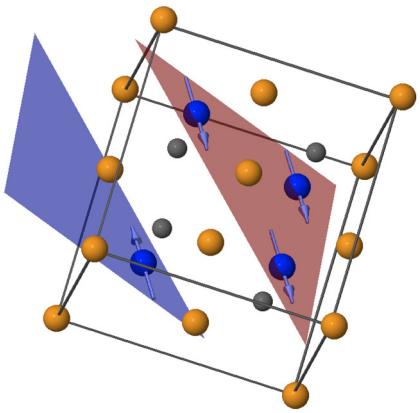

FIG. 1. (Color online) The Gd atoms are shown in black (blue), the Bi as gray (gray), and the Pt as white (yellow). The spins on the Gd atoms are oriented in ferromagnetic planes which are stacked antiferromagnetically along the magnetic propagation vector $(\frac{1}{2}\frac{1}{2}\frac{1}{2})$.

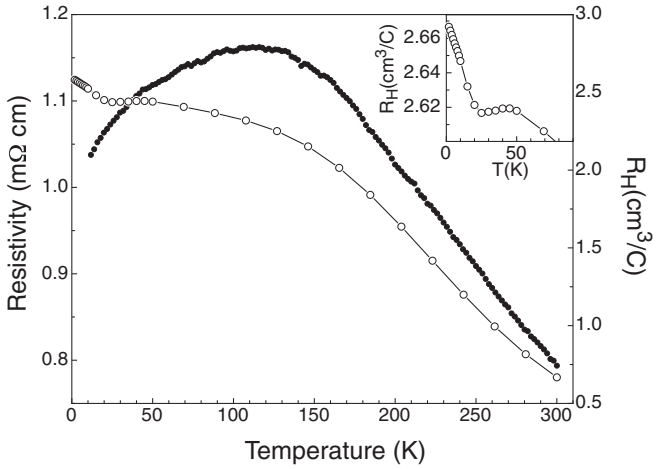

FIG. 2. The solid points show the resistivity $\rho(T)$ of GdBiPt at zero magnetic field for a temperature range of 10–300 K. The open circles show the temperature evolution of the Hall coefficient from 1.8 to 300 K, revealing a kink well above the 9 K Néel temperature (shown in more detail in the inset).

shows a magnetic structure very similar to the one proposed in [7], with the magnetic moments arranged in ferromagnetic sheets, perpendicular to the [111] space diagonal. This makes GdBiPt a strong candidate for this new state of matter.

GdBiPt crystallizes in the cubic half-Heusler crystal structure with the space group $F\bar{4}3m$ [13]. Members of the REBiPt family show many interesting properties such as superconductivity, antiferromagnetic order, and super-heavy-fermion behavior. Band structure calculations and angle-resolved photoemission spectroscopy experiments on Lu, Nd, and GdBiPt [14] indicate the presence of metallic surface states that differ strongly from the band structure in the bulk. However, the authors found that within their resolution an even number of bands cross the Fermi level at the surface, making these states sensitive to disorder unlike in strong topological insulators where an odd number of crossings is expected, protecting surface states from being backscattered by a nonmagnetic impurity. An x-ray resonant magnetic scattering (XRMS) study on GdBiPt indicated a doubling of the unit cell along its [111] space diagonal, however, the authors were unable to establish the exact direction of the magnetic moments [15], information that is essential in determining whether GdBiPt could be an AFTI.

The half-Heusler structure consists of four interpenetrating fcc lattices shifted by $[\frac{1}{4},\frac{1}{4},\frac{1}{4}]$, three of them occupied by a different element while the fourth forms an ordered vacancy. We carried out combined refinement of our x-ray and neutron scattering data, which yields the lowest χ^2, if the atoms in GdBiPt take the same positions as reported for YbBiPt [16] and CeBiPt [17]—platinum located on the [0,0,0] site ($4a$), Gd^{3+} on the $[\frac{1}{4},\frac{1}{4},\frac{1}{4}]$ ($4c$), and Bi on the $[\frac{3}{4},\frac{3}{4},\frac{3}{4}]$ position ($4d$) (see Table I of [18]). These atomic positions are in agreement with the ones that have been previously reported by Kreyssig *et al.* [15]. In addition, we also carried out a single crystal x-ray diffraction experiment. Due to the noncentrosymmetric nature of the $F\bar{4}3m$ space group, we also tested an inverted structure (racemic twin) with Pt on the $4a$, Bi on the $4c$, and Gd on the $4d$ site in order to see if such a structure could account for the observed intensities. In a noncentrosymmetric structure, anomalous x-ray scattering leads to different intensities for so-called *Friedel* pairs, such as (hkl) and $(\bar{h}\bar{k}\bar{l})$. The refinement confirmed the original structure, resulting in R1 = 0.0241, where R1 is the difference between the experimental observations and the ideal calcluated values, and a Flack parameter, which is the absolute structure factor, of −0.13(2) for the current structure in contrast to R1 = 0.0806 and Flack parameter of 1.2(1) for the inverted structure (please note that a Flack parameter is 0 for the correct structure and 1 for the inverted structure).

GdBiPt has a low carrier density ($\sim 3 \times 10^{18}$ cm^{-3}/C). Figure 2 shows that there is a gradual increase in the Hall coefficient as the temperature is reduced, with a clear kink near 25 K. The Hall coefficient was measured using a Quantum Design PPMS, which was also used for the specific heat measurements. CeBiPt also shows such a kink followed by a stronger increase of R_H. In CeBiPt this kink appears at the transition temperature T_N and was ascribed to the development of a superzone gap in the ordered state and consequently a reduction of the number of charge carriers [19]. In GdBiPt a similar kink seems to be present: however, it occurs around 25 K which is above $T_N \sim 9$ K.

For a temperature range of 50–300 K, the magnetic susceptibility χ of Gd^{3+} shows a Curie-Weiss behavior with a Curie-Weiss temperature θ_W of −31.5(3) K, and an effective magnetic moment μ_{eff} of 7.97(4)μ_B consistent with the 7.94μ_B expected for Gd^{3+}. The data were taken in an applied field of 0.05 T using a Quantum Design VSM squid magnetometer. The magnetic entropy S_{mag} shown as the dashed line reaches $0.9R$ ln(8) at T_N indicative of the absence of frustration in contrast to the predictions of [20]. Here S_{mag} was calculated by integrating the magnetic specific heat $C - C_{ph} - C_{el}$ after subtracting the phonon C_{ph} and electronic contributions C_{el}, respectively. Figure 3 also shows that $\frac{d}{dT}(\chi T)$ exhibits a peak at 8.5 K which confirms the antiferromagnetic ordering with a Néel temperature T_N of 8.5 K. In fact, all three measurements—specific heat $C_p(T)$, electrical resistivity $\frac{d}{dT}\rho(T)$ (not shown), as well as the

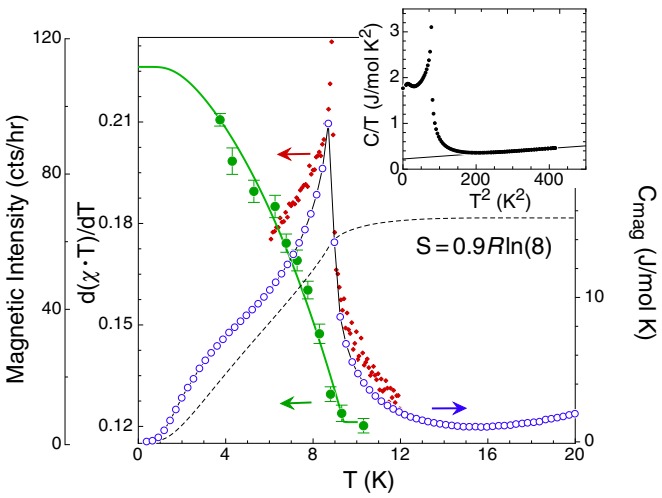

FIG. 3. (Color online) Inset: The specific heat is shown as C/T vs T^2. The solid line is a fit to determine the phonon contribution $C_{\rm ph} = \beta T^3$ and the electronic specific heat $C_{\rm el} = \gamma T$. Main figure: The open circles show the magnetic specific heat $C_m = C - C_{\rm ph} - C_{\rm el}$; solid diamonds show the temperature derivative of the magnetic susceptibility $\frac{d}{dT}(\chi T)$. Solid green circles show the intensity of the first magnetic peak $(\frac{1}{2}\,\frac{1}{2}\,\frac{1}{2})$ plotted as a function of temperature. The solid line is a fit to the square of the magnetic moment, obtained from numerically solving a Weiss model for a J of $\frac{7}{2}$.

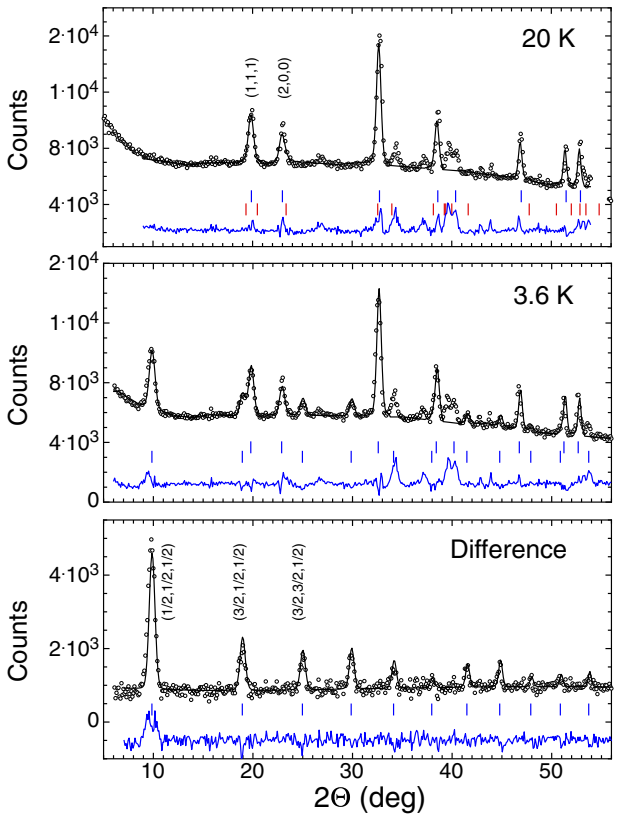

FIG. 4. (Color online) Neutron powder diffraction patterns for GdBiPt taken above (20 K, top panel) and below (3.6 K, middle panel) the Néel temperature. The bottom panel emphasises the form of the magnetic scattering by showing the difference between the 20 K and 3.6 K patterns. The solid line through the data is a fit (described in the text) while the solid line below each pattern shows the residuals. In the 20 K pattern (top), the upper set of Bragg markers are for the nuclear contribution from GdBiPt. The second row indicates the position of Bi flux. In the 3.6 K pattern (middle), the first row of Bragg markers is the nuclear contribution, and the bottom row is the magnetic contribution. As the difference pattern (bottom) only has magnetic peaks, the Bragg markers are for the magnetic pattern.

magnetic susceptibility $\frac{d}{dT}(\chi T)$—show discontinuities at the same critical temperature $T_{\rm N}$, giving evidence to the high quality of our samples [21,22].

At fit to a straight line of C/T as a function of T^2 for temperatures above 15 K yields a $C_{\rm ph} = \beta T^3$ with a β of $2.9(2) \times 10^4$ J/mol K^4. This value of β corresponds to a Debye temperature $\theta_{\rm D}$ of 188(5) K. The same fit results in a Sommerfeld coefficient γ of only 2 mJ/mol K^2, which is low for a metallic compound containing heavy elements such as Gd and Bi. In contrast, the heavy fermion YbBiPt shows a γ of 8 J/mol K^2, which was assigned to low lying crystal field levels [16]. Since in GdBiPt the angular momentum L of the $4f^7$ configuration is zero, crystal fields are not expected to play a significant role. Consequently, we should observe the full magnetic moment of the Gd^{3+} ion. This is supported by the 0.9 R ln(8) entropy release observed in the phase transition.

Our GdBiPt crystals were grown from nonenriched Gd containing the natural abundance of the different Gd isotopes which lead to an extreme absorption cross section of GdBiPt [23]. In order to still be able to carry out our neutron diffraction experiment, we used a thinly dispersed sample on a large flat Si sample plate with a very low background (for details, see [18,23]). The neutron diffraction pattern in the top panel of Fig. 4 was taken at 20 K, well above the Néel temperature. It therefore shows only nuclear reflections which can be indexed with the MgAsAg-type fcc structure. On cooling below $T_{\rm N}$ to 3.6 K the gadolinium moments order and several magnetic reflections appear in the middle panel of Fig. 4. All of the magnetic peaks can be indexed as $(\frac{2n-1}{2}\,\frac{2n-1}{2}\,\frac{2n-1}{2})$ with $n = 1,2,\ldots,$ indicating that the magnetic unit cell is doubled along the (1 1 1) direction of the crystallographic unit cell.

Plotting the intensity of the first magnetic peak against temperature (Fig. 3) and fitting it reveals a Néel temperature of 9.4(1) K, slightly higher than derived earlier from heat capacity and susceptibility. The **k** vector $\mathbf{k}_1 = [\frac{1}{2},\frac{1}{2},\frac{1}{2}]$ of this type-II antiferromagnetic structure belongs to a star containing three more elements $\mathbf{k}_2 = [-\frac{1}{2},\frac{1}{2},\frac{1}{2}]$, $\mathbf{k}_3 = [-\frac{1}{2},-\frac{1}{2},\frac{1}{2}]$, and $\mathbf{k}_4 = [\frac{1}{2},-\frac{1}{2},\frac{1}{2}]$, which are equivalent due to the cubic symmetry. We then used the BASIREPS program, which is part of the FULLPROF suite [24]) to find the basis functions of the irreducible representations of the $F\bar{4}3m$ space group with $\boldsymbol{k}$=$[\frac{1}{2}\,\frac{1}{2}\,\frac{1}{2}]$. This symmetry allows two sets of basis functions whose real and imaginary components are listed in Table I.

For the basis functions listed in Table I the magnetic moment is given by

$$\mathbf{S} = C[\mathbf{BasR} + i\mathbf{BasI}]. \qquad (1)$$

The two basis functions of set 2 represent the two racemic structures possible. Due to the fact that we used powder these

TABLE I. Real (BASR) and imaginary (BASI) components of the basis vectors for the two permitted commensurable magnetic structures obtained from BASIREPS for the space group $F\bar{4}3m$, an ordering wave vector **k** of $[\frac{1}{2},\frac{1}{2},\frac{1}{2}]$, and Gd^{3+} sitting on the 4*c* crystallographic site.

	Set 1	Set 2	
BASR	(1 1 1)	(1 −0.5 −0.5)	(−0.5 1 −0.5)
BASI	(0 0 0)	(0 −0.866 0.866)	(−0.866 0 0.866)

are indistinguishable in the refinement and we are left with a single parameter *C* as a refinable quantity.

The first set of basis functions places the gadolinium moments along the body diagonal of the cubic structure. However, the $(\frac{1}{2}\ \frac{1}{2}\ \frac{1}{2})$ peak is forbidden for this set since three of the four equivalent $(\frac{1}{2}\ \frac{1}{2}\ \frac{1}{2})$ peaks are systematically absent due to the translational symmetry of the space group (face centered), and the fourth is absent due to the magnetic polarization factor for neutron scattering. However, it is clear from the difference pattern in Fig. 4 that this is the strongest of the observed magnetic peaks. This allows us to rule out the first set of basis functions.

A refinement of the second set of basis functions contains two equivalent basis vectors, of which the first was chosen for the refinement. The 3.6 K pattern returns a Gd magnetic moment of $6.6(7)\mu_B$ which corresponds to a moment of $7.6(5)\mu_B$ at 0 K, which is comparable to value of $7.55\mu_B$ reported for single crystal Gd [25]. The difference pattern in Fig. 4 was also refined and gave the same $6.7(6)\mu_B$ for the Gd moment at 3.6 K.

Previous resonant magnetic x-ray scattering experiments [15], were unable to determine the direction of the magnetic moment of GdBiPt. Their attempts to refine the actual moment direction were inconclusive as they had several sizable magnetic domains within the $\sim 0.5 \times 0.5$ mm^2 beam footprint that led to incomplete averaging over directions. By working with a powder and a much larger ($\sim 2.5 \times 8$ cm^2) beam footprint, domain averaging is complete in our data permitting a full analysis of the peak intensities and allowing us to determine the magnetic structure. Complex (e.g., cycloidal) ordering was deemed to be incompatible with the XRMS data [15], and since we detected no other magnetic scattering down to $2\theta = 4^\circ$ ($q \sim 0.33$ Å^{-1}), we can directly rule out long-period modulations of the magnetic structure with periods less than about 19 Å (about three lattice spacings). Longer-period modulations would yield satellites around the magnetic peaks which are also absent. We conclude that GdBiPt adopts a simple collinear type-II antiferromagnetic structure. The magnetic unit cell is eight times larger than the crystallographic unit cell, as the $\boldsymbol{k} = [\frac{1}{2}\ \frac{1}{2}\ \frac{1}{2}]$ propagation vector doubles all three crystallographic axes. The magnetic moments form ferromagnetic sheets which are stacked antiferromagnetically along the [111] body diagonal (Fig. 1). The same propagation vector is found for the vanadium doped half-Heusler compound CuMnSb [26], but not for CeBiPt which orders as a type-I antiferromagnet with a propagation vector of [100] [17]. The evaluation of the magnetic moment direction with the program BASIREPS suggests a common, single **k**-vector structure with the moments perpendicular to the space diagonal. Our results make GdBiPt a strong candidate material for an AFTI.

The results presented here suggest a similar structure to that proposed by Mong *et al.* [7], with an observed spin arrangement that results in strong spin-orbit interaction along the space diagonal. This leads to a path asymmetry for interferromagnetic plane hopping between nonmagnetic sites. In conclusion, given its spin structure, GdBiPt is therefore a promising candidate for an antiferromagnetic topological insulator.

The research at McGill and UdeM received support from the Natural Sciences and Engineering Research Council of Canada (Canada) and Fonds Québécois de la Recherche sur la Nature et les Technologies (Québec). A.D.B. and Y.M. are also supported by the Canada Research Chair Foundation. The neutron diffraction measurements were made at the Canadian Neutron Beam Centre, Chalk River, Ontario.

[1] K. Klitzing, G. Dorda, and M. Pepper, Phys. Rev. Lett. **45**, 494 (1980).
[2] D. J. Thouless, M. Kohmoto, M. P. Nightingale, and M. den Nijs, Phys. Rev. Lett. **49**, 405 (1982).
[3] C. L. Kane and E. J. Mele, Phys. Rev. Lett. **95**, 146802 (2005).
[4] B. A. Bernevig, T. L. Hughes, and S.-C. Zhang, Science **314**, 1757 (2006).
[5] J. E. Moore, Nature (London) **464**, 194 (2010).
[6] M. Z. Hasan and C. L. Kane, Rev. Mod. Phys. **82**, 3045 (2010).
[7] R. S. K. Mong, A. M. Essin, and J. E. Moore, Phys. Rev. B **81**, 245209 (2010).
[8] C. Fang, M. J. Gilbert, and B. A. Bernevig, Phys. Rev. B **88**, 085406 (2013).
[9] S. Chadov, X. Qi, J. Kübler, G. H. Fecher, C. Felser, and S. C. Zhang, Nat. Mater. **9**, 541 (2010).
[10] H. Lin, L. A. Wray, Y. Xia, S. Xu, S. Jia, R. J. Cava, A. Bansil, and M. Z. Hasan, Nat. Mater. **9**, 546 (2010).
[11] D. Xiao, Y. Yao, W. Feng, J. Wen, W. Zhu, X.-Q. Chen, G. M. Stocks, and Z. Zhang, Phys. Rev. Lett. **105**, 096404 (2010).
[12] W. Al-Sawai, H. Lin, R. S. Markiewicz, L. A. Wray, Y. Xia, S.-Y. Xu, M. Z. Hasan, and A. Bansil, Phys. Rev. B **82**, 125208 (2010).
[13] P. C. Canfield, J. D. Thompson, W. P. Beyermann, A. Lacerda, M. F. Hundley, E. Peterson, Z. Fisk, and H. R. Ott, J. Appl. Phys. **70**, 5800 (1991).
[14] C. Liu, Y. Lee, T. Kondo, E. D. Mun, M. Caudle, B. N. Harmon, S. L. Bud'ko, P. C. Canfield, and A. Kaminski, Phys. Rev. B **83**, 205133 (2011).
[15] A. Kreyssig, M. G. Kim, J. W. Kim, D. K. Pratt, S. M. Sauerbrei, S. D. March, G. R. Tesdall, S. L. Bud'ko, P. C. Canfield, R. J. McQueeney *et al.*, Phys. Rev. B **84**, 220408 (2011).

[16] R. A. Robinson, A. Purwanto, M. Kohgi, P. C. Canfield, T. Kamiyama, T. Ishigaki, J. W. Lynn, R. Erwin, E. Peterson, and R. Movshovich, Phys. Rev. B **50**, 9595 (1994).

[17] J. Wosnitza, G. Goll, A. D. Bianchi, B. Bergk, N. Kozlova, I. Opahle, S. Elgazzar, M. Richter, O. Stockert, H. V. Löhneysen *et al.*, New J. Phys. **8**, 174 (2006).

[18] See Supplemental Material at http://link.aps.org/supplemental/10.1103/PhysRevB.90.041109 for details of the sample growth, mounting of the sample for the powder neutron diffraction, and details of the x-ray diffraction, as well as the refinement of the crystal and magnetic structure.

[19] M. H. Jung, T. Yoshino, S. Kawasaki, T. Pietrus, Y. Bando, T. Suemitsu, M. Sera, and T. Takabatake, J. Appl. Phys. **89**, 7631 (2001).

[20] S. Khmelevskyi, Phys. Rev. B **86**, 104429 (2012).

[21] M. E. Fisher and J. S. Langer, Phys. Rev. Lett. **20**, 665 (1968).

[22] M. E. Fisher, Philos. Mag. **7**, 1731 (1962).

[23] D. H. Ryan and L. M. D. Cranswick, J. Appl. Crystallogr. **41**, 198 (2008).

[24] J. Rodríguez-Carvajal, Physica B **192**, 55 (1993).

[25] G. Will, R. Nathans, and H. A. Alperin, J. Appl. Phys. **35**, 1045 (1964).

[26] M. Halder, S. M. Yusuf, A. Kumar, A. K. Nigam, and L. Keller, Phys. Rev. B **84**, 094435 (2011).